CSIRO PUBLISHING

Environ. Chem.
http://dx.doi.org/10.1071/EN15154

Research Paper

Arsenic adsorption onto aluminium-substituted goethite

Ana E. Tufo,[A] *María dos Santos Afonso*[B] *and Elsa E. Sileo*[B,C]

[A]Laboratorio de Química Ambiental, 3iA–ECyT, Universidad de San Martín, Martín de Irigoyen 3100, CP1650, Buenos Aires, Argentina.
[B]Instituto de Química Física de los Materiales, Medio Ambiente y Energía, Departamento de Química Inorgánica, Analítica y Química Física, Facultad de Ciencias Exactas y Naturales, Universidad de Buenos Aires, Pabellón II, Ciudad Universitaria, C1428EHA, Buenos Aires, Argentina.
[C]Corresponding author. Email: e_sileo@yahoo.es

Environmental context. Goethite, commonly found in soils, is often partially substituted by Al and strongly influences the mobility of arsenic in the environment. The adsorption of As^V onto goethites with increasing Al substitution was explored, finding that Al incorporation decreases As^V sorption per gram of adsorbent, and that a low level of Al incorporation enhances the adsorption per unit area. Structures of the complexes formed between As^V and the oxy(hydr)oxide surface, at different pH values, are proposed by studying the changes in the surface charges of the adsorbed and non-adsorbed substituted and non-substituted goethites.

Abstract. Aluminium and iron oxy(hydr)oxides in nature are often partially substituted by other elements and strongly influence the mobility of arsenic in the environment. Because goethite is commonly found in soils, and the oxide is easily substituted, in the present work, the adsorption of As^V onto several Al-substituted goethites was explored in order to determine how substitution affects the adsorption process. Three samples with increasing Al content (GAl_0, $GAl_{3.78}$ and $GAl_{7.61}$) were prepared and fully characterised. The variations in As^V adsorption under different conditions, as well as the variations of the particle surface charge, were analysed. The results showed that the removal capacity of Al-goethites is determined by the Al content. The adsorption maxima per gram followed the trend $GAl_0 > GAl_{3.78} > GAl_{7.61}$, indicating that Al incorporation decreases As^V sorption. Adsorption per surface area decreased in the order $GAl_{3.78} > GAl_0 > GAl_{7.61}$, implying that a small incorporation of Al enhances the adsorption properties of the surface. The stoichiometry of the probable surface complexes formed with the contaminant at different pH values is proposed, by analysis of all the experimental results obtained before and after As^V adsorption. These surface complexes were used to fit the experimental data with good agreement, and the formation and acidity constants were also estimated.

Additional keywords: Al-goethite, zeta potential.

Received 18 July 2015, accepted 21 March 2016, published online 5 May 2016

Introduction

Arsenic is a ubiquitous metalloid that presents a serious risk to the health of humans, animals and plants.[1,2] Although arsenic is present in only $\sim 5 \times 10^{-5}$ % by weight on the Earth's crust,[3] different arsenic-containing species may be concentrated in some reducing marine sediments or sedimentary rocks. The mobilisation of As^V in nature results mainly from weathering reactions, biological activity and volcanic emissions, followed by water-mediated transport through the environment,[4] and anthropogenic mobilisation from varied human activities.[5,6]

Arsenite (AsO_3^{3-}, As^{III}) and arsenate (AsO_4^{3-}, As^V) ions are the two common arsenic species found in natural environments. Both species present different toxicity, As^{III} being more toxic, soluble and mobile than As^V at certain pH values.[7] The oxidation state of As^V highly depends on the redox and pH conditions of the media,[8] and several mechanisms have been invoked to explain arsenic mobility.[9] Such mechanisms include microbial reduction of As^V in anaerobic environments,[10] dissimilatory reductive dissolution of Fe^{III} oxy(hydr)oxides that may lead to the release of adsorbed arsenic into the aqueous phase,[11] and competition of solutes for sorption sites on iron oxides.[9]

Under oxidising conditions, As^V is the predominant form, and previous studies have revealed that the ion is associated primarily with the Fe^{III} oxy(hydr)oxide coatings of soil particles, or is strongly adsorbed onto clays, manganese oxides and (hydr)oxides and organic matter.[5]

Among soil components, goethite and ferrihydrite are commonly found. Both minerals exhibit a hydroxylated surface that presents a strong affinity for anions,[12] cations[12,13] or organic molecules.[14] In particular, arsenic species are sorbed onto these oxy(hydr)oxides and their mobility is highly influenced,[15–17] controlling the arsenic biogeochemical cycle.

The adsorption of arsenic on iron oxides is pH-dependent, and Pierce and Moore[18] reported that As^V is preferentially sorbed onto Fe oxy(hydr)oxides between pH 4 and 7, whereas As^{III} is preferentially sorbed between pH 7 and 10.

Several studies, including X-ray absorption spectroscopy (XAS), neutron diffraction, high-resolution transmission electron microscopy (HRTEM) and density functional theory (DFT) molecular modelling, have revealed that arsenic may form a large variety of arsenic surface complexes on sorption onto ferric oxy(hydr)oxides and oxides. In particular, Fendorf et al. explored the structure of the surface complexes formed with As^V, reporting three different Fe–As distances of 0.285, 0.324 and 0.360 nm.[19] These distances were assigned to the presence of bidentate mononuclear edge-sharing (2E), bidentate binuclear corner-sharing (2C) and monodentate mononuclear corner-sharing (1V) complexes. Some years later, using DFT calculations, Sherman and Randall[20] reported that the 2C complex is substantially more favoured energetically over the hypothetical 2E mononuclear complex. Using X-ray absorption fine structure EXAFS spectroscopy (EXAFS), these authors also showed that the peak near 0.285 nm results from As–O–O–As multiple scattering and not from an As–Fe backscatter, and indicated that the distance at 0.326 nm corresponded to the bidentate binuclear complex. The presence of the monodentate mononuclear complexes was not confirmed in the same work. Several recent studies have also proposed that the 2E complexes do not form in the case of the adsorption of tetrahedral As^V species onto goethite.[21–23] This bidentate mononuclear complex appears to be specific to As^{III} complexes. Ona-Nguema et al. studied the adsorption of arsenite onto 2-line ferrihydrite, haematite, goethite and lepidocrocite,[24] finding that the adsorption onto haematite and ferrihydrite is similar, but differs significantly from that on goethite and lepidocrocite. The main difference is the absence of a 2E complex at the surface of the last two minerals.

In addition to these three types of surface complexes, tridentate hexanuclear corner-sharing (3C) surface complexes have also been proposed by analysing the adsorption of As^{III} onto iron spinels. In these inner-sphere complexes, AsO_3 pyramids occupy vacant tetrahedral sites on the octahedrally terminated {111} surfaces of magnetite[22,25] and maghemite,[26] which explains, in part, the high adsorption affinity of arsenite for these substrates.

Recent important findings provide evidence for the formation of both outer-sphere and inner-sphere As^V complexes at the haematite–aqueous solution boundary, and Catalano et al. reported that ~35 % of the adsorbed arsenic occurred in the outer-sphere form in the haematite samples studied.[27] The exact nature of these outer-sphere complexes is still poorly understood, but the fact that they are not displaced with increasing ionic strength suggests that they could correspond to hydrogen-bonded species. Such outer-sphere complexes are difficult to detect using EXAFS spectroscopy in the presence of inner-sphere As^V complexes.[28]

The adsorption of As^V onto goethite was also studied in artificial seawater by Gao and Mucci,[29] who reported that the presence of Mg^{II} and Ca^{II} enhanced As^V adsorption at pH > 7.0. The authors also determined that at pH < 6.5, arsenate adsorption is well reproduced using the constant capacitance model with the inclusion of ternary complexes.

The upper layer of lateritic soils is dominated by goethite and haematite, and when these minerals are formed in terrestrial weathering environments, they usually exhibit Al-for-Fe substitution. Al incorporation leads to changes in particle size, and goethite crystals become smaller as Al substitution increases. The crystals also change from multiple-domain to single-domain ones. The effect of Al incorporation on the surface area of the particles depends on the level of incorporation, because aluminium reduces both the rate of growth and the crystal size, with the final surface area depending on which of these effects prevails.[30] These variations in surface areas alter the adsorption properties of the oxy(hydr)oxide. As an example of the influence of Al substitution on adsorption properties, Masue et al. demonstrated that As^V adsorption onto coprecipitated aluminium : iron oxy(hydr)oxides decreases as the Al : Fe molar ratio increases.[31]

Conversely, Silva et al. compared the potential of As^V adsorption of pure goethite and three Al-goethites with different Al contents.[32] The authors found that Al incorporation considerably enhanced the As^V uptake per gram of goethite, and concluded that Al-goethites are good potential adsorbents to remove As^V from water. However, it must be emphasised that the authors tested solids with very different surface areas, and that this difference in areas causes the enhancement in the As^V uptake when it is expressed per gram of adsorbent.

Arsenic sorption onto Al-goethite is often found in nature, and the process is an economical and reliable technique and an efficient method for the removal of inorganic compounds. In the present study, the adsorption of As^V onto three samples of pure and Al-substituted goethites was re-explored on several goethites prepared following the same procedure. The results revealed that the specific surface areas of the goethites vary between 20 and 36 $m^2\ g^{-1}$.

The samples obtained were fully characterised, and the effect of pH on the adsorption of As^V was investigated. The variations in surface electric charge (zeta potential, ZP) before and after arsenic sorption, and at different pH values, were also analysed to propose a stoichiometry of the surface complexes formed.

Materials and methods

Adsorbents

Samples of pure and Al-substituted goethites were prepared following the method of Schwertmann and Cornell,[33] by aging mixtures of 5 M KOH and different volumes of 1 M $Fe(NO_3)_3$ and 0.5 M $Al(NO_3)_3$ solutions at 70 °C, in the appropriate volume ratio to yield the required μ_{Al} ($\mu_{Al} = [Al] \times 100/([Al] + [Fe])$, [Al] and [Fe], mol L^{-1}). Samples containing nominal μ_{Al} values of 0.0, 8.00 ± 0.02 and 27.00 ± 0.02 were prepared and aged for 24 days in the basic solution. The final μ_{Al} values were 0, 3.78 and 7.61 respectively, and samples were named GAl_0, $GAl_{3.78}$ and $GAl_{7.61}$, where the subindex refers to the final μ_{Al} in the sample. To remove poorly crystalline iron compounds from pure goethite, the solid was extracted in the dark with ammonium oxalate (0.2 M, pH 3.00) for 4 h. To remove extra Al from the Al-containing samples, the solids were washed twice with 400 mL 1 M KOH, and the final pH was adjusted to 7.50 with 1 M HCl. The precipitates obtained were washed, dialysed until the conductivity of the solution was similar to that of doubly distilled water, and dried at 50 °C for 48 h. Reagent-grade chemicals were used. In all experiments, solutions were prepared with high-purity 18 MΩ cm water.

Adsorbent characterisation

Chemical and physical analyses of the solids

The iron content in the synthesised materials was determined spectrophotometrically using the thioglycolic acid method.[34] The Al content was measured by inductively coupled plasma (ICP) atomic emission spectrometry using a Shimadzu ICPS-1000 III apparatus (Nakagyo-ku, Kyoto, Japan).

The attenuated total reflection Fourier-transform infrared (ATR-FTIR) spectra of solids were recorded on a FTIR Nicolet 8700 spectrometer equipped with a HgCdTe (MCT) detector and a Balston H_2O/CO_2 stripper (MCT/B) detector, in the 400–4000 cm^{-1} region, with a resolution of 1 cm^{-1}. A horizontal boat plate (Spectra Tech) with a ZnSe 45° crystal was used as the internal reflection element (IRE). FTIR spectra were the result of 1024 co-added interferograms.

Thermogravimetric analysis (TGA) for all samples was performed on a Shimadzu TGA-51 under an inert atmosphere of N_2(g) at a flow rate of 20 mL min^{-1}. A ramp of 6 °C min was used from room temperature to 500 °C. The mass of solid used was 20 mg.

Specific surface areas (SSAs) were determined by N_2(g) adsorption–desorption experiments at 77 K, using a manometric adsorption apparatus (AccuSorb 2100, Micrometrics). The measurements were conducted on solids previously outgassed at 60 °C, and higher outgassing temperatures were avoided to prevent phase changes in the samples. The SSAs were obtained by the Brunauer–Emmett–Teller (BET) method,[35] using a relative pressure range of 0.05–0.25.

Rietveld refinement of X-ray diffraction data and crystal morphology

X-ray diffraction (XRD) patterns were obtained with a Cu target tube and a diffracted beam graphite monochromator. XRD patterns were measured in the 2θ range 17.5–130°, in 0.025° steps, using 8 s as counting time. The data were analysed using the *GSAS* system,[36] with the *EXPGUI* interface.[37] The mean coherence path dimensions (MCP) or crystallite sizes were determined in the parallel direction (L_{paral}) and perpendicular direction (L_{perp}) to the anisotropic broadening (110) axis. Starting unit-cell parameters and atomic coordinates for goethite were taken from the literature,[38] and peak profiles were fitted using the Thompson–Cox–Hastings pseudo-Voigt function.[39] Crystallite dimensions were calculated making allowances for the instrument broadening function, which had been previously modelled using lanthanum hexaboride as a standard reference material. Particle morphology and size were characterised using scanning electron microscopy (SEM) by examining a drop of suspension dried onto a metallic support (Zeiss Supra 40, field emission, gun-scanning electron microscope).

Adsorption experiments

All the adsorption and kinetic experiments were performed in triplicate, and the experimental error within each replicate was less than 5 %. The reported values correspond to the average of the results obtained.

Effect of Al concentration on arsenic adsorption kinetics

The sorption of As^V was measured on samples GAl_0, $GAl_{3.78}$ and $GAl_{7.61}$ as a function of reaction time. The suspensions were prepared from solids hydrated by 30-min sonication before the addition of the sorbates. The experiments were conducted at pH 5.50 ± 0.02 and 25.00 ± 0.02 °C, under a N_2 atmosphere, in magnetically stirred thermostat-coupled double-jacket cells with perforated stoppers provided with pH and temperature sensors. The pH values of individual samples were adjusted during the experiments by adding 0.1 M KOH or 0.1 M HNO_3 (Mettler T70 automatic titrator). The solid samples (0.1000 g) were placed in contact with arsenate solutions (50 mL, 0.53 mM) prepared by dissolving analytical-grade disodium hydrogen arsenate heptahydrate ($Na_2HAsO_4.7H_2O$, Merck) in Milli-Q water. KNO_3 (0.1 M) was used as background electrolyte for all the experiments. Approximately 15 aliquots of 1 mL each were withdrawn from the dispersion during each run and syringe-filtered using a 0.22-μm-pore cellulose acetate membrane. Depending on the concentration range, arsenic concentrations were measured spectrophotometrically using the molybdenum blue method,[40] or by ICP atomic emission spectrometry (Shimadzu ICPS-1000 III).

Adsorption isotherms

To obtain the adsorption isotherms (mmol of As^V adsorbed *v.* different As^V equilibrium concentrations), batch experiments were carried out for 2 h at pH 5.50 ± 0.20 and 25.00 ± 0.02 °C. The experimental set-up was the same as that used for the kinetic measurements, and the As^V concentration was varied between 0.03 and 0.53 mM.

Effect of pH on arsenic adsorption

The adsorption capacity of the solids was plotted *v.* pH values (range 4.00 to 8.00) to construct the adsorption envelopes. The experimental set-up was the same as that used for the kinetic measurements. The pH was adjusted during the whole measurement time, and the initial arsenic concentration was 0.53 mM in all experiments. Blank tests containing As^V in solution were used to measure the amount of arsenic adsorbed by the walls of the reaction vessels, but corrections were unnecessary.

Point of zero charge determinations

The point of zero charge (PZC) of each adsorbent, before and after As^V adsorption, was determined using a Zeta Plus light-scattering zeta potential analyser (Brookhaven Instruments Co.). The measurements were performed by adding 0.05 g of each solid to 1000 mL 0.1 M KNO_3 solution. The solution/solid ratio used was equal to 20 L g^{-1}, and the suspensions were equilibrated for 24 h. The PZC values of the arsenate adsorbed solids were measured on samples exposed to an initial As^V concentration of 0.53 mM, and corresponded to those with maximum adsorption capacity ($GAl_0 = 0.0018$, $GAl_{3.78} = 0.0026$ and $GAl_{7.61} = 0.0017$ mmol m^{-2}). The pH values were adjusted by adding 0.1 M KOH or HNO_3, and the pH values were varied between 3.00 and 10.00.

Results and discussion

Chemical and physical analyses of the solids

The preparative and final contents of Al^{III} in the samples are listed in Table 1. The maximum incorporation of Al, expressed as μ_{Al} and reached in 20 days, was 7.61 ± 0.02, indicating that only part of the aluminium present was incorporated into the solid. As was mentioned before, the iron and aluminium amorphous phases present in the solids were removed by treatment with ammonium oxalate or KOH. Then, the rinsed samples were analysed by ATR-FTIR and TGA. The interferograms showed that only the characteristic bands of goethite due to δ(OH) and γ(OH) vibrations (891 and 793 cm^{-1} respectively) were present in the three samples. These band frequencies shifted to higher values as Al incorporation increased. No oxalate bands were detected on the surface of the samples (Fig. S1 in the Supplementary material). The TGAs also showed the absence of oxalate adsorbed onto the samples

Table 1. Metal content, results of the Rietveld refinement, specific surface areas (SSAs) and point of zero charge (PZC) values for pure and Al-substituted goethites

Sample	GAl_0	$GAl_{3.78}$	$GAl_{7.61}$
μ_{Al} (preparative)	0.00	8.00 ± 0.02	27.00 ± 0.02
μ_{Al} (final)	0.00	3.78 ± 0.02	7.61 ± 0.02
SSAs ($m^2\ g^{-1}$)	36 ± 1	20 ± 1	25 ± 1
PZC values	5.36 ± 0.27	4.46 ± 0.22	4.58 ± 0.23
a (Å)	4.6132(2)	4.6108(2)	4.6019(1)
b (Å)	9.9598(2)	9.9364(2)	9.9093(2)
c (Å)	3.0246(1)	3.0186(1)	3.0104(1)
Cell volume (Å^3)	138.975(8)	138.298(8)	137.282(5)
L_{perp} (nm)	420	800	334
L_{paral} (nm)	37	45	64

(Fig. S2 in the Supplementary material). The crystallographic characterisation and BET areas are discussed later.

Crystal morphology

Goethite crystals display a multitude of shapes and sizes; however, the basic morphology is essentially acicular.[41] Frequently, particles consist of parallel subunits or domains that extend along the *c* axis and are stacked along the *a* and *b* axes. SEM micrographs taken at 400 000× and 600 000× (Fig. S3 in the Supplementary material) showed the formation of acicular platelets. Pure goethite (GAl_0) exhibited the longest particles (average size 903×110 nm). The average dimensions in the Al-goethites changed with the Al content (515×88 nm in $GAl_{3.78}$ to 484×80 nm in $GAl_{7.61}$), indicating that the width-to-length ratio of the particles was greater in the Al-goethites and increased in the more Al-concentrated samples. The micrograph at 600 000× magnification showed that particles result from the piling up of smaller particles, which form noticeable pores on the surface.

Rietveld refinement of XRD data and SSAs

The XRD patterns showed anisotropic broadening of the peaks and the displacement of the peaks towards higher 2θ values with Al incorporation (Fig. S4 in the Supplementary material). Goethite was the only crystalline phase found. The results of the Rietveld simulation (Tables 1 and Table S1 in the Supplementary material) indicated that the unit cell parameters (*a*, *b* and *c*) and consequently the cell volume decreased with Al content, confirming the effective Al-for-Fe substitution. Calculated MCP dimensions, reflecting the crystallite size in the parallel (L_{paral}) and perpendicular (L_{perp}) directions to the normal to plane (110), varied with the Al content. L_{perp} increased with a low Al content, but a greater content made its value decrease. In contrast, L_{paral} increased along the series. These coherence lengths are related to the propagation distance over which the dispersed wave is coherent and are consequently related to the order of the crystal. The calculated values indicated that $GAl_{3.78}$ showed the largest crystallite size. The decreasing particle sizes observed by SEM micrographs (Fig. S3) and the MCP dimensions obtained by Rietveld refinement (Table 1) showed that Al inclusion increases the nucleation rate, leading to the formation of smaller individual crystals with varied crystallinity.

The effect of Al incorporation on the SSAs of goethites varied with the Fe-for-Al substitution and followed the trend GAl_0 $(36 \pm 1) > GAl_{7.61}$ $(25 \pm 1) > GAl_{3.78}$ $(20 \pm 1\ m^2\ g^{-1})$.

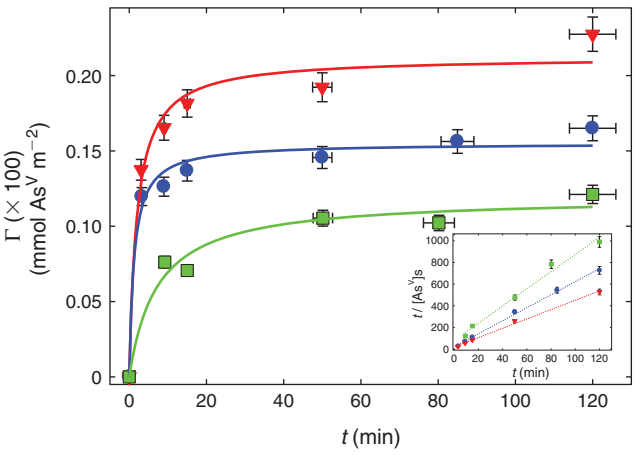

Fig. 1. As^V sorbed (Γ, mmol m^{-2}) onto the different goethites *v.* time at pH 5.50 and 25.00 °C. GAl_0, blue circles; $GAl_{3.78}$, red triangles; $GAl_{7.61}$, green squares (average values from three independent measurements). Solid lines correspond to the fitting of the data to the pseudo-second-order rate kinetic model.

This order did not match the particle size obtained by SEM but followed the same sequence of crystallite size of the samples (MCP dimensions), where samples GAl_0 and $GAl_{3.78}$ showed the largest and smallest BET areas (36 and 20 $m^2\ g^{-1}$), and the smallest and highest crystallinity.

Effect of Al substitution on arsenic adsorption kinetics

The experiments on adsorption of As^V were conducted for 120 min at pH 5.50 ± 0.02 and 25.00 ± 0.02 °C under a N_2 atmosphere, using 0.53 mM arsenate ($H_xAsO_4^{3+x}$). The results are presented in Fig. 1 and show an almost constant value of the sorption process after 2 h, followed by a slight increase that is probably indicative of a binding to 'hidden' sites in the pore space between domains.

The amount of As^V adsorbed by the sorbent (mmol m^{-2}) at equilibrium is expressed as Γ and is calculated as:

$$\Gamma = \frac{C_o - C_f}{m \times a}$$

where C_o, C_f, *m* and *a* are the initial concentration of As^V, the concentration of As^V at different times, and the adsorbent mass and surface area respectively.

Several kinetic models were used to fit the data, but the pseudo-second-order rate equation[42] presented the best agreement with the experimental results. This model has been widely used to describe metal cation and oxyanion sorption on different sorbents. The pseudo-second-order kinetic rate equation is expressed as:

$$\frac{t}{C_f} = \frac{1}{k\Gamma^2} + \frac{t}{\Gamma} \quad (1)$$

where Γ is the amount of As^V sorbed at equilibrium expressed in millimoles per metre squared, *k* is the rate constant of sorption (m^2 $mmol^{-1}$ min^{-1}) and C_f is the amount of As^V sorbed on the surface of the solid (mmol m^{-2}) at different times, *t* (min).

The experimental data followed the equation, and straight lines were obtained when t/C_f was plotted *v.* *t*, revealing that the

Table 2. Kinetic data, kinetic constants (k) and correlation coefficients values for the sorption of As^V onto the samples at pH 5.50

Sample	GAl_0	$GAl_{3.78}$	$GAl_{7.61}$
pH value	5.50 ± 0.20	5.50 ± 0.20	5.50 ± 0.20
$k \times 10^2$ (m^2 $mmol^{-1}$ min^{-1})	5.204 ± 1.025	2.371 ± 0.078	1.117 ± 0.048
$[As^V]_{s,eq} \times 10^3$ (mmol As^V m^{-2})	1.6 ± 0.1	2.1 ± 0.1	1.2 ± 0.1
R^2	0.984	0.983	0.972
P	<0.01	<0.01	<0.01

process follows the proposed rate equation (inset in Fig. 1). The results of the fitting (Table 2) indicated that the rate constants decrease with increase in Al incorporation. At pH 5.50, the $k \times 10^2$ values obtained were 5.204 ± 1.025, 2.371 ± 0.078 and 1.117 ± 0.048 m^2 $mmol^{-1}$ min^{-1} for samples GAl_0, $GAl_{3.78}$ and $GAl_{7.61}$ respectively. The values indicated that an increase of μ_{Al} by a factor of 2 leads to a decrease of k by the same factor, showing that k is inversely proportional to the Al content, displaying slower kinetics. Under these experimental conditions, the maximum $\Gamma \times 10^3$ adsorbed when the equilibrium is reached followed the trend $GAl_{3.78}$ $(2.1 \pm 0.1) > GAl_0$ $(1.6 \pm 0.1) > GAl_{7.61}$ (1.2 ± 0.1) when the results are expressed per metre squared, and GAl_0 $(58.6 \pm 0.1) > GAl_{3.78}$ (42.8 ± 0.1) $> GAl_{7.61}$ (30.4 ± 0.1) when expressed per gram of adsorbent.

The results indicated that pure goethite adsorbs As^V more efficiently and more rapidly than Al-goethites. The fit of the experimental results to the second-order equation may indicate that the controlling rate process is chemical sorption involving chemical bonding forces between adsorbent and adsorbate and suggesting inner-sphere complex formation.[43]

Adsorption isotherms

Arsenic(V) adsorption isotherms reached a maximum and constant value at ~0.45 mM (Fig. 2). The available sorption sites of the surface at this concentration are saturated.

The adsorption isotherms were modelled using the single-site Langmuir equation,

$$\Gamma = \frac{\Gamma_{max}[As^V]_{eq}K_L}{(1 + K_L[As^V]_{eq})} \quad (2)$$

where Γ and Γ_{max} are the amount of As^V adsorbed by the sorbent (mmol m^{-2}) at equilibrium and saturation respectively, $[As^V]_{eq}$ is the equilibrium concentration of As^V remaining in solution (mM), and K_L is the constant related to the energy of adsorption (L $mmol^{-1}$). This model assumes one type of reaction site, monolayer coverage and no change in affinity with sorption density. Experimental data presented a good fit to the Langmuir equation, with correlation coefficient (R^2) values in the range 0.932–0.995 (Fig. 2 and Table 3).

The Γ_{max} values (mmol m^{-2} and mmol g^{-1}) varied in the order: $GAl_{3.78}$ (0.0026) > GAl_0 (0.0018) ≈ $GAl_{7.61}$ (0.0017) and GAl_0 (0.065) > $GAl_{3.78}$ (0.053) > $GAl_{7.61}$ (0.044) respectively, indicating that the incorporation of Al enhances the adsorption of As^V per unit area only in the more diluted sample.

The value of arsenate adsorption on the pure sample (0.0018 mmol m^{-2}) was in agreement with the data obtained by O'Reilly et al.,[44] Liu et al.[45] and Antelo et al.,[46] who reported values in the range 1.9 to 2.5×10^{-3} mmol m^{-2} at pH

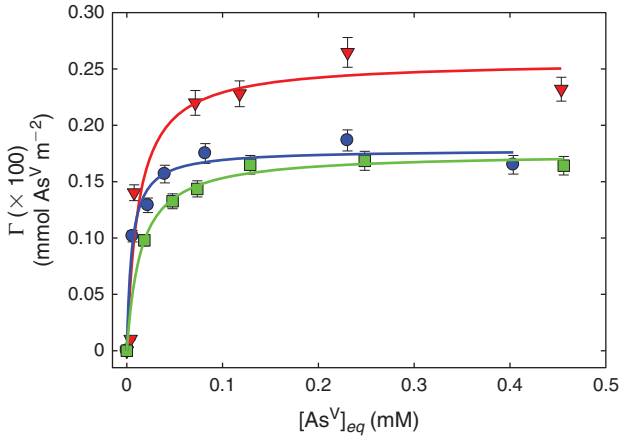

Fig. 2. As^V adsorbed onto pure and Al-substituted goethites normalised by surface area at pH 5.50. Solid lines are the fitting of the averaged data to Langmuir's equation in the range 0.03–0.53 mM. GAl_0, blue circles; $GAl_{3.78}$, red triangles; $GAl_{7.61}$, green squares.

Table 3. Maximum adsorption coverage (Γ_{max}), adsorption constants (K_L), and determination coefficients (R^2) of the Langmuir function for the adsorption of As^V onto the prepared goethites

Sample	Γ_{max} (mmol m^{-2})	Γ_{max} (mmol g^{-1})	K_L (L $mmol^{-1}$)	R^2	P
GAl_0	0.0018 ± 0.0001	0.065 ± 0.002	188.67 ± 4.17	0.984	<0.01
$GAl_{3.78}$	0.0026 ± 0.0002	0.053 ± 0.004	81.97 ± 2.13	0.932	<0.01
$GAl_{7.61}$	0.0017 ± 0.0001	0.044 ± 0.001	68.49 ± 8.33	0.995	<0.01

below neutrality. However, it must be taken into account that a direct comparison between values reported by different authors is not always feasible because the experiments are often run under different conditions (adsorption time, temperature, pH and ionic strength). Moreover, as the anion adsorption strongly depends on PZC values, it must be emphasised that we performed the sorption on a goethite sample displaying a low PZC value of 5.36.

In order to explore the influence of Al presence on the As^V sorption properties of the oxy(hydr)oxide, we also performed identical adsorption experiments on samples of pure natural diaspore (α-AlOOH) using a similar contact time to the one used for pure goethite (120 min). The mineral was fully characterised (Figs S5, S6 in the Supplementary material), and As^V sorption on diaspore was markedly low, indicating that the adsorption kinetics are slower than for iron minerals. Additionally, the As^V sorption on diaspore reached a coverage of 0.019 mmol g^{-1} after 24 h. This value is markedly lower than the values reported by O'Reilly et al. (0.192 mmol g^{-1}) for pure goethite exposed to As^V for 24 h,[44] and by Huang et al. for boehmite (0.133 mmol g^{-1}),[47] and showed the low adsorption capacity of the mineral.

Adsorption is a surface phenomenon and its extent depends on different surface parameters such as particle size, surface roughening, porosity and crystallite size among others. The particle surface could be described using the Terrace–Ledge–Kink (TLK) model. This model describes the thermodynamics of crystal surface formation, transformation and growth as well as the energetics of surface defect formation, surface diffusion, vaporisation and adsorption.[48]

As mentioned before, the effect of Al incorporation on the surface area of the particles depends on the level of incorporation, because aluminium reduces both the rate of growth and the crystal size, with the final surface area depending on which of these effects prevails.[30] These variations in surface area could alter the adsorption properties of the oxy(hydr)oxide because they change not only the relative distribution of each kind of surface site but also the identity of the surface site. The Gibbs free energy for the adsorption process (ΔG_{ads}) is the sum of the binding energies of each site and is a measure of reaction spontaneity. Thus, ΔG_{ads} will depend not only on the ligand identity but also on the characteristics of the adsorption active sites, and their number, availability and structure.

The amount of As^V adsorbed per gram onto the partially substituted goethites decreased with Al incorporation and agreed with the data found for diaspore.

The data obtained also indicated that, when expressed by unit area, the incorporation of Al enhances the adsorption of As^V only in the more diluted sample, probably owing to a higher number of defective sites available on the surface of this sample.

Our results agree with the work of Masue et al.,[31] who studied the adsorption of As^V onto coprecipitated Al : Fe oxy (hydr)oxides, but the data are not in agreement with the results of Silva et al., who concluded that Al-goethites are good sorbents for the contaminant without considering that they compared pure goethite with a low surface area (20.6 $m^2\ g^{-1}$) and Al-goethites with high surface areas (124.7–113.2 $m^2\ g^{-1}$), and high Al contents (μ_{Al} values in the range 13–23).[32] In the present work, solids with similar areas are compared, and it is demonstrated that, when expressed per gram of adsorbent, Al incorporation decreases the adsorption of As^V. Regarding adsorption expressed per unit area, the results of Silva et al. are in agreement with our findings because they did not explore the diluted Al-goethites[32] that were studied in the present work.

An analogous conclusion was published by Martin et al.,[49] who also used goethite and Al-goethite with similar surface area to adsorb As^V. In this case, the μ_{Al} value of this Al-goethite was 10, and the adsorption at comparable pH and solution concentration followed a similar trend, with a decrease of the As^V surface concentration to 0.079 mmol m^{-2}. This adsorption coverage value is close to the adsorption coverage of diaspore mentioned above (0.019 mmol g^{-1} or 0.073 mmol m^{-2}).

In general, the stability constants for aluminium complex formation are at least 10 times lower than for iron complex formation. ΔG_{ads} is directly related to the stability constants of the surface complexes, and under similar aqueous solution conditions, coverage is lower. As was mentioned before, the adsorption kinetics on Al-goethites are slower than on pure goethites with higher activation energies. Thus, the reaction is less spontaneous and more impaired with higher energy requirements.

Although the empirical K_L value has little significance as a theoretical chemical binding constant, this constant is rather useful for assessing the comparative adsorption behaviour of different materials.[50] The K_L values obtained (188.67 ± 4.17; 81.97 ± 2.13; 68.49 ± 8.33 L $mmol^{-1}$) indicated that pure goethite presents a higher arsenate affinity than Al-goethites, and even though $GAl_{3.78}$ showed an intermediate K_L value (81.97 ± 2.13 L $mmol^{-1}$), the removal of As^V (m^{-2}) by $GAl_{3.78}$ is the most effective in the series. Because no reasons related to chemical equilibrium theory supported the increase of adsorption in $GAl_{3.78}$, the observed behaviour can only be ascribed to the overall change undergone by the solid surface with the incorporation of small quantities of Al, which evidently increases the number of surface reactive sites.

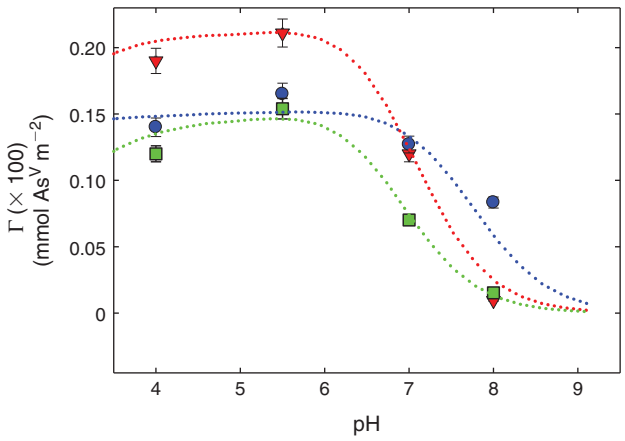

Fig. 3. Effect of pH on As^V sorption onto samples: GAl_0, blue circles; $GAl_{3.78}$, red triangles; $GAl_{7.61}$, green squares. These experiments were performed in triplicate at 25.00 °C, the mass of oxides was 0.100 g and the As^V initial concentration was 0.53 mM. All symbols are experimental averaged data from several independent measurements; dotted lines were calculated from Eqns 3–12 and data in Table 4.

Effect of pH on arsenic adsorption

The effect of pH on the adsorption of arsenic onto samples GAl_0, $GAl_{3.78}$ and $GAl_{7.61}$ was studied with an initial concentration of 0.53 mM (Fig. 3).

As can be seen in Fig. 3, all samples displayed an almost constant adsorption value in the pH range 4.00–6.00 where the monovalent As^V anion, $H_2AsO_4^-$, is the predominant species. After this, in the pH range 6.00–9.00, adsorption decreases.

The decrease in the adsorption curve was displaced to lower pH values in the Al-goethites. These results agree with data previously reported.[29,31,32]

The differences between As^V adsorption onto the samples may also be seen in Fig. 3. For instance, the value $\Delta\Gamma = \Gamma_{GAl_{3.78}} - \Gamma_{GAl_0}$ (difference between the As^V adsorbed at equilibrium onto $GAl_{3.78}$ and GAl_0, mmol m^{-2}) is 0.0005 at pH 4.00, and −0.0007 at pH 8.00. This indicates that at low pH, adsorption onto Al-goethite is higher than onto the pure sample; however, the behaviour is inverted at higher pH. However, the $\Delta\Gamma$ values for sample $GAl_{7.61}$ are −0.0002 at pH 4.00, and −0.0007 at pH 8.00, indicating that pure goethite adsorbs more As^V than the more substituted sample over the whole pH range.

PZC determinations

Zeta potential measurements (ZP) were also conducted before and after the As^V adsorption experiments. These measurements are related to the movement of suspended particles under the influence of an electric field, where the direction of the movement depends on the particle charge. The pH of the solution highly influences the charge of the particles, and the pH value at which the oxide particles do not move under the applied electric field is called the point of zero charge, PZC. Before As^V sorption, the PZC values were observed at pH 5.36, 4.46 and 4.58 for GAl_0, $GAl_{3.78}$ and $GAl_{7.61}$ respectively (Fig. 4). Below these pH values, the goethite particles are predominantly positively charged and above them, negatively charged.

The measured PZC for pure goethite is low when compared with other reported values,[31,32] but it agrees with the values

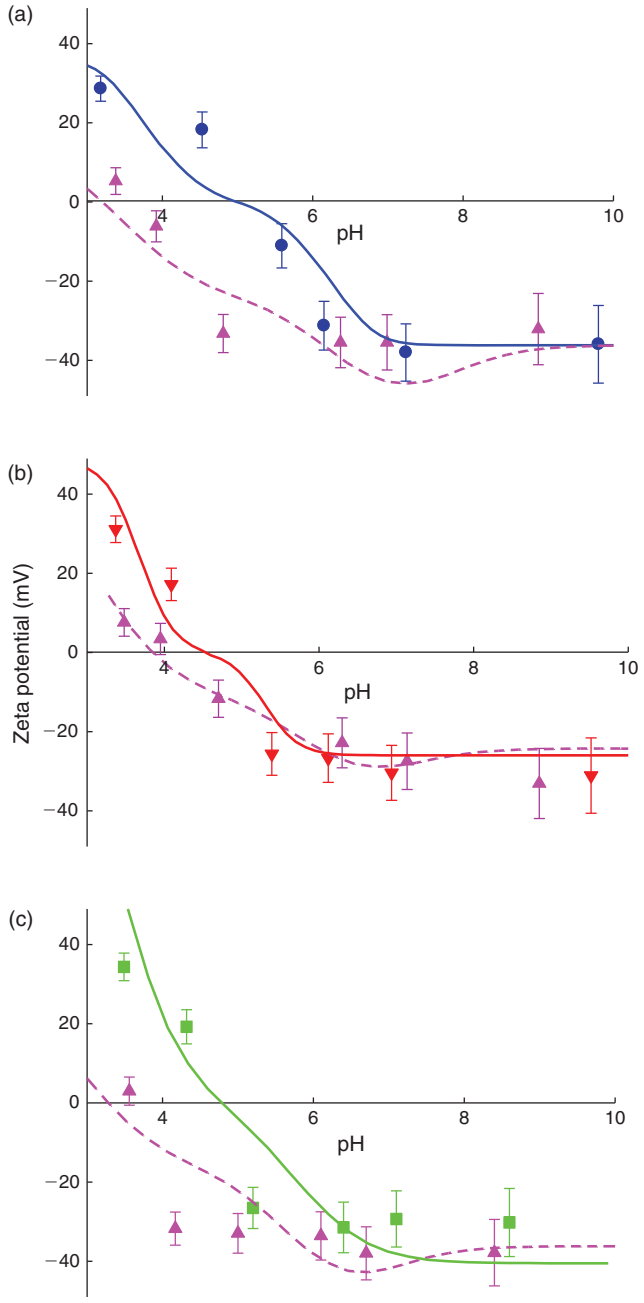

Fig. 4. Zeta potential *v.* pH for the As-loaded (pink dashed line) and -unloaded (solid line) samples. (a) GAl_0; (b) $GAl_{3.78}$; and (c) $GAl_{7.61}$. All symbols are experimental averaged data from several independent measurements, solid and dashed lines were calculated from Eqns 3–12 and data in Table 4. As^V concentration was 0.53 mM.

measured for goethites prepared following similar procedures.[51] Van Schuylenborgh and Arens[52] ascribed this low PZC value to the synthetic procedure where the suspension was aged for several days in strongly basic media, which caused the coprecipitation of OH groups during the slow formation of goethite.

The PZC values of the Al-goethites (4.46 and 4.58 for $GAl_{3.78}$ and $GAl_{7.61}$ respectively) are lower than that of pure goethite, indicating an increase in surface OH groups with the incorporation of the substituting cation. The ZP values at a fixed pH also changed, and noticeable differences were found between the pure and the Al-substituted samples. These differences are related to variations in the number of surface charges and to the different basicity of Fe–OH and Al–OH surface groups. For instance, at pH 5.50, the measured ZP values for GAl_0, $GAl_{3.78}$ and $GAl_{7.61}$ are −9.44, −26.01 and −29.97 mV, indicating that the surface of GAl_0 is less negative than that of samples $GAl_{3.78}$ and $GAl_{7.61}$. At high pH values, the differences are smaller, and error bars in Fig. 4 indicate that they are practically negligible.

Unexpectedly, the PZC value for $GAl_{3.78}$ is lower than that of $GAl_{7.61}$, indicating that the surface charge of the samples did not change monotonously with Al incorporation, and that a small incorporation of Al caused the exposure of a higher number of active sorption centres.

After the loading with As^V and at low pH, the ZP of GAl_0 showed very different ZP values when compared with the unloaded sample (Fig. 4a). For instance, at pH 5.00, the ZP values for the two samples are −33.90 and 8.18 mV, indicating an increase of the negative surface charges in the loaded sample. However, at higher pH, both solids displayed similar constant ZP values, indicating that new negative or positive charges were not formed on the surface on adsorption. This agrees with the expected low adsorption of As^V at high pH values.

Similarly, the PZC also decreased from 5.36 to 3.72 ($\Delta PZC = 1.64$), showing the increment in the surface negative charge with the loading of As^V. The result agrees with previous data that reported a PZC decrease for goethite and gibbsite due to arsenate adsorption.[32,53–57]

Taking into account that the reactive surface centres may be represented as ≡FeOH, which are protonated ($\equiv FeOH_2^+$) at $pH < pH_{PZC}$, and deprotonated ($\equiv FeO^-$) at $pH > pH_{PZC}$,[58] the observed variations in the PZC of the As^V-loaded pure goethite (Fig. 4a) may be explained in terms of the different surface complexes formed with $H_2AsO_4^-$.

In order to describe the changes in ZP values observed in Fig. 4, the nature of the possible surface complexes formed will be discussed.

First, the monodentate mononuclear complexes that As^V may form on the iron sites will be analysed. These may be non-charged or negatively charged complexes of the type

$$\equiv FeOH_2^+ + H_2AsO_4^- \leftrightarrow \equiv FeOAsO_3H_2^0 + H_2O \quad (3a)$$

$$\equiv FeO^- + H_2AsO_4^- \leftrightarrow \equiv FeOAsO_3H^- + OH^- \quad (3b)$$

$$\equiv FeO^- + H_2AsO_4^- \leftrightarrow \equiv FeOAsO_3^{2-} + H_2O \quad (3c)$$

The formation of these complexes reduces the positive surface charge (PSC) by one unit (Eqn 3a), leaves the surface charge unaltered (Eqn 3b), or reduces the negative surface charge (NSC) by one unit (Eqn 3c).

Second, bidentate mononuclear complexes of the following type may also be created

$$\equiv FeOH_2^+ + H_2AsO_4^- \leftrightarrow \equiv FeO_2AsO_2H^- + H_2O + H^+ \quad (4a)$$

$$\equiv FeO^- + H_2AsO_4^- \leftrightarrow \equiv FeO_2AsO_2H^- + OH^- \quad (4b)$$

The formation of the bidentate mononuclear complex (Eqn 4a) decreases the PSC by two units, whereas the formation described by Eqn 4b leaves the surface charge unaltered.

Finally, the bidentate binuclear complexes may also be formed,

$$2 \equiv FeOH_2^+ + H_2AsO_4^- \leftrightarrow (\equiv FeO)_2AsO_2H^0 + 2H_2O + H^+ \quad (5a)$$

$$2 \equiv FeO^- + H_2AsO_4^- \leftrightarrow (\equiv FeO)_2AsO_2^- + 2OH^- \quad (5b)$$

where the PSC is reduced by two units (Eqn 5a), or where the NSC is reduced by one unit (Eqn 5b).

In the case of GAl_0, the decline in ZP observed at low pH (in the predominance zone of $\equiv FeOH_2^+$) after arsenic sorption may be ascribed to the formation of a non-charged monodentate mononuclear complex (Eqn 3a, reduction of PSC by one unit) and to the formation of bidentate mononuclear or bidentate binuclear complexes (reduction of PSC by two units, Eqn 4a, 5a). At $6.00 < pH < 8.00$ (in the predominance zone of $\equiv FeO^-$), the negative ZP values reach a plateau that may be originating from the formation of negatively charged monodentate mononuclear or bidentate mononuclear complexes (Eqns 3b, 3c, 4b) that maintain the total surface charge of the As^V-loaded samples when compared with that of the unloaded samples. At higher pH values, the adsorption is negligible.

In the middle range, $4.50 < pH < 7.00$, the acid–base dissociation equilibrium of the monodentate mononuclear surface complex must also be taken into account, and results in a displacement of the ZP values towards more negative values because of the increase in the NSC:

$$\equiv FeOAsO_3H_2^0 \leftrightarrow \equiv FeOAsO_3H^- + H^+ \quad (6)$$

$$\equiv FeOAsO_3H^- \leftrightarrow \equiv FeOAsO_3^{2-} + H^+ \quad (7)$$

In the case of the less Al-substituted sample $GAl_{3.78}$, the PZC decreased from 4.46 to 3.98 ($\Delta PZC = 0.48$) after As^V adsorption (Fig. 4b), and the ZP values of the adsorbed and non-adsorbed samples differed at low pH but were quite similar at high pH, reaching similar negative values at pH ~5.20. The behaviour may also be explained in terms of the surface complexation model, where the following equilibrium equations of the aluminium centres ($\equiv AlOH$) must also be considered:

$$\equiv AlOH_2^+ + H_2AsO_4^- \leftrightarrow \equiv AlOAsO_3H_2^0 + H_2O \quad (8a)$$

$$\equiv AlO^- + H_2AsO_4^- \leftrightarrow \equiv AlOAsO_3H^- + OH^- \quad (8b)$$

$$\equiv AlO^- + H_2AsO_4^- \leftrightarrow \equiv AlOAsO_3^{2-} + H_2O \quad (8c)$$

$$\equiv AlOH_2^+ + H_2AsO_4^- \leftrightarrow \equiv AlO_2AsO_2H^- + H_2O + H^+ \quad (9a)$$

$$\equiv AlO^- + H_2AsO_4^- \leftrightarrow \equiv AlO_2AsO_2H^- + OH^- \quad (9b)$$

$$2 \equiv AlOH_2^+ + H_2AsO_4^- \leftrightarrow (\equiv AlO)_2AsO_2H^0 + 2H_2O + H^+ \quad (10a)$$

$$2 \equiv AlO^- + H_2AsO_4^- \leftrightarrow (\equiv AlO)_2AsO_2^- + 2OH^- \quad (10b)$$

At low pH values, the loaded sample displays positive ZP values that decrease with the increase of pH. The reduction in surface positive charge may be ascribed to monodentate mononuclear complex (Eqns 3a, 8a) and bidentate binuclear complex formation (Eqns 5a, 10a) onto both iron and aluminium surface centres, where the contribution of negatively charged complexes is negligible ($pH < PZC$). The constant ZP values reached at higher pH may be ascribed to Eqns 4b and 9b.

Finally, the decline in ZP values observed in the middle pH range can be explained by both the dissociation equilibrium of the Fe (Eqns 6, 7) and the Al surface groups:

$$\equiv AlOAsO_3H_2^0 \leftrightarrow \equiv AlOAsO_3H^- + H^+ \quad (11)$$

and

$$\equiv AlOAsO_3H^- \leftrightarrow \equiv AlOAsO_3^{2-} + H^+ \quad (12)$$

which increase the NSC, displacing the ZP to more negative values.

The most Al-substituted goethite, $GAl_{7.61}$, presented a PZC that decreased from 4.58 to 3.67 ($\Delta PZC = 0.91$) on As^V adsorption (Fig. 4c). At low pH, the differences in ZP between the loaded and unloaded samples are smaller than in GAl_0, and as in the case of sample $GAl_{3.78}$, the changes in ZP may be ascribed to the formation of the different surface complexes.

In order to obtain the intrinsic surface complexation constants involved in Eqns 3–12, and using the surface protonation and deprotonation constants obtained for each sample from its PZC value (see below), and initial constant values reported previously,[59] the experimental data *v.* pH were modelled at 0.1 M ionic strength. The results obtained are displayed in Table 4 and as dotted lines in Fig. 3.

$$pH_{(pzc)} = 1/2(pK_{a1} + pK_{a2})$$

where K_{a1} and K_{a2} are the acidity constants.

In order to estimate the values of the equilibrium constants, the type and properties of the reactive sites and the charge distribution in the particle were taken into account, and the electrical double layer model (which describes the charge distribution and the decay of the potential on the aqueous side of the interface) was used. The values of the net charges were fairly well approximated using the ZP data.

To improve the quality of the refined data, the obtained constants were re-refined by fitting the measured zeta potential *v.* pH values shown in Fig. 4. The theoretical calculated ZP values are also displayed as dashed lines in the same figure. The log *K* obtained values for the following equations were 3.94 and −2.16.

$$\equiv FeOH + H_2AsO_4^- \leftrightarrow \equiv FeO_2AsO(OH)^- + H_2O$$

$$\equiv FeOH + H_2AsO_4^- \leftrightarrow \equiv FeO_2AsO_2^{2-} + H_2O + H^+$$

Within experimental error, these values coincide with the ones reported by Jeppu and Clement (3.56 and −2.73).[59]

In contrast, the log *K* value for the following equation was 7.44.

$$\equiv FeOH + H_2AsO_4^- + H^+ \leftrightarrow \equiv FeOAsO_3H_2^0 + H_2O$$

This value was not in agreement with the data reported by Jeppu and Clement,[59] who found a value of 9.05. This difference

Table 4. Aqueous protonation and intrinsic surface complexation constants for As^V adsorption on GAl_0, $GAl_{3.78}$ and $GAl_{7.61}$ at 0.1 M ionic strength

Chemical reaction	log *K*		
	GAl_0	$GAl_{3.78}$	$GAl_{7.61}$
$\equiv FeOH + H^+ \leftrightarrow \equiv FeOH_2^+$	3.72	3.72	3.72
$\equiv FeOH \leftrightarrow \equiv FeO^- + H^+$	−7.00	−7.00	−7.00
$\equiv FeOH + H_2AsO_4^- + H^+ \leftrightarrow \equiv FeOAsO_3H_2^0 + H_2O$	7.44	5.15	5.74
$\equiv FeOH + H_2AsO_4^- \leftrightarrow \equiv FeOAsO_3H^- + H_2O$	3.94	3.64	3.49
$\equiv FeOH + H_2AsO_4^- \leftrightarrow \equiv FeOAsO_2^{2-} + H_2O + H^+$	−2.16	−2.06	−1.96
$2 \equiv FeOH + H_2AsO_4^- + H^+ \leftrightarrow (\equiv FeO)_2AsO_2H^0 + 2H_2O$	13.64	12.34	12.54
$\equiv AlOH + H^+ \leftrightarrow \equiv AlOH_2^+$	–	4.00	4.10
$\equiv AlOH \leftrightarrow \equiv AlO^- + H^+$	–	−7.78	−7.70
$\equiv AlOH + H_2AsO_4^- + H^+ \leftrightarrow \equiv AlOAsO_3H_2^0 + H_2O$	–	4.04	4.64
$\equiv AlOH + H_2AsO_4^- \leftrightarrow \equiv AlOAsO_3H^- + H_2O$	–	2.54	2.39
$\equiv AlOH + H_2AsO_4^- \leftrightarrow \equiv AlOAsO_3^{2-} + H_2O + H^+$	–	−3.15	−3.05
$2 \equiv AlOH + H_2AsO_4^- + H^+ \leftrightarrow (\equiv AlO)_2AsO_2H^0 + 2H_2O$	–	11.24	11.45

results from assuming the formation of the surface complex $(\equiv FeO)_2AsO_2H^0$ throughout the equation:

$$2 \equiv FeOH + H_2AsO_4^- + H^+ \leftrightarrow (\equiv FeO)_2AsO_2H^0 + 2H_2O$$

which was not considered by Jeppu and Clement.[59] This complex could be the predominant one based on the value of log *K*.

The refining allowed the calculation of the following acidity constants formed on the surfaces of GAl_0, $GAl_{3.78}$ and $GAl_{7.61}$ respectively

$$\equiv FeOAsO_3H_2^0 \quad \leftrightarrow \equiv FeOAsO_3H^- + H^+$$

where $p^sK_{a1} = 3.50$, 1.51 and 2.25, and

$$\equiv FeOAsO_3H^- \leftrightarrow \equiv FeOAsO_3^{-2} + H^+$$

where $p^sK_{a2} = 6.10$, 5.70 and 5.45 respectively.

It is interesting to note that the calculated p^sK_{a2} values for $\equiv FeOAsO_3H^-$ are slightly lower than that of $H_2AsO_4^-$ ($pK_a = 6.96$), indicating that this iron surface complex is more acidic than $H_2AsO_4^-$. The values obtained are similar to those reported for several inorganic anions (SO_4^{-2}, SeO_4^{-2}, SO_3^{-2}) that form inner-sphere complexes.[60]

The acidity constants on the aluminium sites were also calculated, showing similar values to the ones found for the iron sites:

$$\equiv AlOAsO_3H_2^0 \leftrightarrow \equiv AlOAsO_3H^- + H^+$$

where $p^sK_{a1} = 1.50$ and 2.25 for $GAl_{3.78}$ and $GAl_{7.61}$, and

$$\equiv AlOAsO_3H^- \leftrightarrow \equiv AlOAsO_3^{-2} + H^+$$

where $p^sK_{a2} = 5.69$ and 5.44 for $GAl_{3.78}$ and $GAl_{7.61}$.

In order to graphically illustrate the variations in the surface change between the loaded and the unloaded samples, we represented the Δ_{ZP} value *v.* pH (Fig. 5):

$$\Delta_{ZP}(mV) = ZP_{loaded} - ZP_{unloaded}$$

This difference gives a clear idea of the surface charge variation caused by the adsorption process. Additionally,

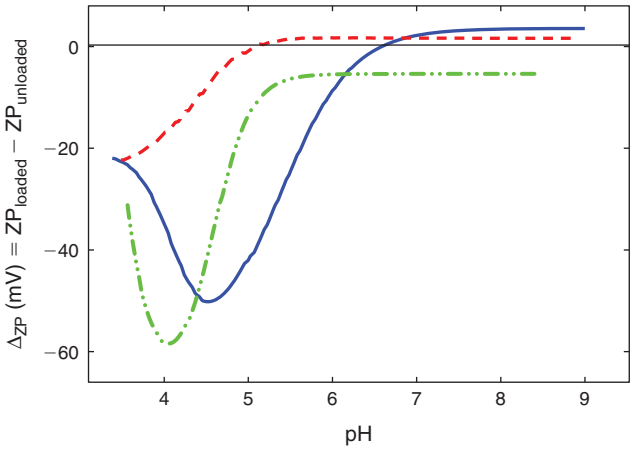

Fig. 5. Difference in zeta potential value between the As-loaded and the unloaded samples Δ_{ZP} *v.* pH; GAl_0, blue solid line; $GAl_{3.78}$, red dashed line; $GAl_{7.61}$ green dot–dashed line.

differences in the ordinate axis are related to the number of surface sites occupied by the charged complexes.

As can be seen in Fig. 5, the curves are similar for GAl_0 and $GAl_{7.61}$ and differ for $GAl_{3.78}$. The clear displacement of the curve to the right for sample $GAl_{3.78}$ cannot be ascribed to Al incorporation but indicates that the sample is intrinsically different from GAl_0 and $GAl_{7.61}$.

At low pH, with surface metal centres $\equiv FeOH_2^+$, samples GAl_0 and $GAl_{7.61}$ show a negative slope, which reveals that the surface is turning more negative (or less positive) by the formation of negatively or zero-charged complexes (Eqns 3a, 4a, 5a, 6, 8a, 9). The number of positive surface groups $\equiv FeOH_2^+$ decreases along the pH range, and the negative charge also increases owing to the presence of labile H^+ on the Al centres. In conclusion, the variations in $ZP_{loaded} - ZP_{unloaded}$ may be explained by the formation of mono- and bidentate complexes.

At pH > 4.52 (for GAl_0) and pH > 4.05 (for $GAl_{7.61}$), where the metal centres may be represented as $\equiv FeO^-$, the slope turned positive, denoting that the formation of negative (and neutral) complexes diminished. The decrease in negative charge may be ascribed to the formation of the monodentate and bidentate binuclear deprotonated complexes (Eqns 3a, 3c, 4a, 5a, 5b, 8a, 8c, 9a, 10a,10b). The formation of the same complexes justifies

the positive slope observed for $GAl_{3.78}$. The bidentate binuclear complexes have already been reported by Ladeira and Ciminelli,[61] who found this type of bond formed on the surface of gibbsite exposed to As^V. The formation of this type of As^V complex is highly relevant to environmental science because bidentate complexes are highly resistant to desorption.

Sample $GAl_{7.61}$ displayed only $\Delta_{ZP} < 0$, indicating that the surface of the unloaded sample is less negative than that of the loaded sample in the whole pH range. The minimum Δ_{ZP} value for $GAl_{3.78}$ is lower than 3.70 (outside the graphic range), and the data indicate that $GAl_{3.78}$ has the least negative (or most positive) surface, followed by $GAl_{7.61}$ and GAl_0 (Figs 4, 5).

The fact that $GAl_{3.78}$ presents the largest coverage does not imply that the sample would present the lowest value in the Δ_{ZP} *v.* pH curve, because the As complexes may be formed without changes in the overall surface charge.

Taking into account that most surface natural waters present pH values in the range 6.00–8.00, the previous results indicate that the surface complexes formed between arsenic and Al-goethites will correspond to $\equiv FeO_2AsO_2H^-$ and $\equiv FeOAsO_3^{-2}$, and similar ones will be formed on aluminium.

Conclusions

Among the most common different arsenic removal technologies, adsorption is one of the most widely used for removing the contaminant from a contaminated source.

Several adsorptive media have been reported to remove arsenic from water, and removal efficiency will depend on the identity of the sorbent and the oxidation state of the arsenic compounds. As^V adsorption capacity per gram of Al-goethites is reduced along the Al-for-Fe substitution gradient, and pure goethite adsorbs As^V more efficiently and more rapidly than Al-goethites, although the behaviour is inverted at higher pH. The incorporation of small amounts of Al enhances the adsorption of As^V per unit area, and the adsorption efficiency decreases when Al concentration in the solid sample increases. The As^V-loaded and the unloaded sample behaviour could be explained by the formation of monodentate mononuclear, bidentate mononuclear and bidentate binuclear surface complexes. Further measurements using other spectroscopy techniques such as EXAFS may be required to elucidate the structure of these surface complexes.

Because of the ubiquity of Al-goethites in the environment, the data presented clarify the role they play in the mobility of As^V in natural waters and soils. Also, the Al-goethites proved to be a poorer candidate than pure goethite as sorbents in As^V removal technologies, but their low cost and easy availability make them a good choice.

Supplementary material

SEM additional figures, XRD diagrams and agreement factors for the Rietveld refinements, FTIR spectra and thermogravimetric analysis data are available online (see http://www.publish.csiro.au/?act=view_file&file_id=EN15154_AC.pdf).

Acknowledgements

The authors acknowledge the Universidad de Buenos Aires (UBA) and Agencia Nacional de Promoción Científica y Tecnológica for financial support through UBACyT and Proyecto de Investigación Científica y Tecnológica grants. The authors are also thankful to the Consejo Nacional de Investigaciones Científicas y Técnicas de la República Argentina (CONICET).

References

[1] B. K. Mandal, K. T. Suzuky, Arsenic around the world: a review. *Talanta* **2002**, *58*, 201. doi:10.1016/S0039-9140(02)00268-0

[2] D. J. Vaughan, Arsenic. *Elements* **2006**, *2*, 71. doi:10.2113/GSELEMENTS.2.2.71

[3] P. Ravenscroft, H. Brammer, K. Richard, *Arsenic Pollution: a Global Synthesis* **2009** (Wiley-Blackwell: Chichester, UK).

[4] J. Bundschuh, P. Bhattacharya, B. Nath, R. Naidu, J. Ng, L. R. G. Guilherme, L. Q. Ma, K.-W. Kim, J. S. Jean, Arsenic ecotoxicology: the interface between geosphere, hydrosphere and biosphere. *J. Hazard. Mater.* **2013**, *262*, 883. doi:10.1016/J.JHAZMAT.2013.08.019

[5] S. Wang, C. N. Mulligan, Natural attenuation processes for remediation of arsenic-contaminated soils and groundwater. *J. Hazard. Mater.* **2006**, *138*, 459. doi:10.1016/J.JHAZMAT.2006.09.048

[6] S. Wang, C. N. Mulligan, Occurrence of arsenic contamination in Canada: sources, behavior, and distribution. *Sci. Total Environ.* **2006**, *366*, 701. doi:10.1016/J.SCITOTENV.2005.09.005

[7] J. Matschullat, Arsenic in the geosphere – a review. *Sci. Total Environ.* **2000**, *249*, 297. doi:10.1016/S0048-9697(99)00524-0

[8] P. L. Smedley, D. G. Kinniburgh, A review of the source, behavior and distribution of arsenic in natural waters. *Appl. Geochem.* **2002**, *17*, 517. doi:10.1016/S0883-2927(02)00018-5

[9] S. Dixit, J. G. Hering, Comparison of arsenic(V) and arsenic(III) sorption onto iron oxide minerals: implications for arsenic mobility. *Environ. Sci. Technol.* **2003**, *37*, 4182. doi:10.1021/ES030309T

[10] R. S. Oremland, T. R. Kulp, J. S. Blum, S. E. Hoeft, S. Baesman, L. G. Miller, J. F. Stolz, A microbial arsenic cycle in a salt-saturated, extreme environment. *Science* **2005**, *308*, 1305. doi:10.1126/SCIENCE.1110832

[11] W. Sun, R. Sierra-Alvarez, L. Milner, R. Oremland, J. A. Field, Arsenite and ferrous iron oxidation linked to chemolithotrophicdenitrification for the immobilization of arsenic in anoxic environments. *Environ. Sci. Technol.* **2009**, *43*, 6585. doi:10.1021/ES900978H

[12] S. Musić, M. Ristic, Sorption of chromium(VI) on hydrous iron oxides. *Z. Wasser Abwasser For.* **1986**, *19*, 186.

[13] S. Musić, M. Ristic, Adsorption of trace elements or radionuclides on hydrous iron oxides. *J. Radioanal. Nucl. Chem.* **1988**, *120*, 289. doi:10.1007/BF02037344

[14] B. C. Barja, M. dos Santos Afonso, Aminomethylphosphonic acid and glyphosate adsorption onto goethite: a comparative study. *Environ. Sci. Technol.* **2005**, *39*, 585. doi:10.1021/ES035055Q

[15] J. Aguilar, C. Dorronsoro, E. Fernández, J. Fernández, I. García, F. Martín, M. Sierra, M. Simón, Remediation of As-contaminated soils in the Guadiamar River Basin (SW, Spain). *Water Air Soil Pollut.* **2007**, *180*, 109. doi:10.1007/S11270-006-9254-3

[16] B. A. Manning, S. E. Fendorf, S. Goldberg, Surface structures and stability of arsenic(III) on goethite: spectroscopic evidence for inner-sphere complexes. *Environ. Sci. Technol.* **1998**, *32*, 2383. doi:10.1021/ES9802201

[17] G. A. Waychunas, B. A. Rea, C. C. Fuller, J. A. Davis, Surface chemistry of ferrihydrite. Part 1. EXAFS studies of the geometry of coprecipitated and adsorbed arsenate. *Geochim. Cosmochim. Acta* **1993**, *57*, 2251. doi:10.1016/0016-7037(93)90567-G

[18] M. L. Pierce, C. M. Moore, Adsorption of arsenite and arsenate on amorphous iron hydroxide. *Water Res.* **1982**, *16*, 1247. doi:10.1016/0043-1354(82)90143-9

[19] S. Fendorf, M. J. Eick, P. Grossl, D. L. Sparks, Arsenate and chromate retention mechanisms on goethite. 1. Surface structure. *Environ. Sci. Technol.* **1997**, *31*, 315. doi:10.1021/ES950653T

[20] D. M. Sherman, S. R. Randall, Surface complexation of arsenic(V) to iron(III) (hydr)oxides: structural mechanism from ab initio molecular geometries and EXAFS spectroscopy. *Geochim. Cosmochim. Acta* **2003**, *67*, 4223. doi:10.1016/S0016-7037(03)00237-0

[21] B. Cancès, F. Juillot, G. Morin, V. Laperche, L. Alvarez, O. Proux, J.-L. Hazemann, G. E. Brown Jr, G. Calas, XAS evidence of As^V association with iron oxyhydroxides in a contaminated soil at a former arsenical pesticide processing plant. *Environ. Sci. Technol.* **2005**, *39*, 9398. doi:10.1021/ES050920N

[22] G. Morin, Y. Wang, G. Ona-Nguema, F. Juillot, G. Calas, N. Menguy, E. Aubry, J. R. Bargar, G. E. Brown, EXAFS and HRTEM evidence for As^{III}-containing surface precipitates on nanocrystalline magnetite: implications for As sequestration. *Langmuir* **2009**, *25*, 9119. doi:10.1021/LA900655V

[23] Y. Wang, G. Morin, G. Ona-Nguema, F. Juillot, F. Guyot, G. Calas, G. E. Brown, Evidence for different surface speciation of arsenite and arsenate on green rust: an EXAFS and XANES study. *Environ. Sci. Technol.* **2010**, *44*, 109. doi:10.1021/ES901627E

[24] G. Ona-Nguema, G. Morin, F. Juillot, G. Calas, G. E. Brown, EXAFS analysis of arsenite adsorption onto two-line ferrihydrite, hematite, goethite, and lepidocrocite. *Environ. Sci. Technol.* **2005**, *39*, 9147. doi:10.1021/ES050889P

[25] Y. Wang, G. Morin, G. Ona-Nguema, N. Menguy, F. Juillot, E. Aubry, F. Guyot, G. Calas, G. E. Brown, Arsenite sorption at the magnetite–water interface during aqueous precipitation of magnetite: EXAFS evidence for a new arsenite surface complex. *Geochim. Cosmochim. Acta* **2008**, *72*, 2573. doi:10.1016/J.GCA.2008.03.011

[26] M. Auffan, J. Rose, O. Proux, D. Borschneck, A. Masion, P. Chaurand, J. L. Hazemann, C. Chaneac, J. P. Jolivet, M. R. Wiesner, A. Van Geen, J. Y. Bottero, Enhanced adsorption of arsenic onto maghemites nanoparticles: As^{III} as a probe of the surface structure and heterogeneity. *Langmuir* **2008**, *24*, 3215. doi:10.1021/LA702998X

[27] J. G. Catalano, C. Park, P. Fenter, Z. Zhang, Simultaneous inner- and outer-sphere arsenate adsorption on corundum and hematite. *Geochim. Cosmochim. Acta* **2008**, *72*, 1986. doi:10.1016/J.GCA.2008.02.013

[28] L. Charlet, G. Morin, J. Rose, Y. Wang, M. Auffan, A. Burnol, A. Fernandez-Martinez, Reactivity at (nano)particle–water interfaces, redox processes, and arsenic transport in the environment. *C. R. Geosci.* **2011**, *343*, 123. doi:10.1016/J.CRTE.2010.11.005

[29] Y. Gao, A. Mucci, Acid–base reactions, phosphate and arsenate complexation, and their competitive adsorption at the surface of goethite in 0.7 M NaCl solution. *Geochim. Cosmochim. Acta* **2001**, *65*, 2361. doi:10.1016/S0016-7037(01)00589-0

[30] D. G. Schulze, U. Schertzmann, The influence of aluminium on iron oxides: XIII. Properties of goethites synthesized in 0.3 M KOH at 25 °C. *Clay Miner.* **1987**, *22*, 83. doi:10.1180/CLAYMIN.1987.022.1.07

[31] Y. Masue, R. H. Loeppert, T. A. Kramer, Arsenate and arsenite adsorption and desorption behavior on coprecipitatedaluminium:iron hydroxides. *Environ. Sci. Technol.* **2007**, *41*, 837. doi:10.1021/ES061160Z

[32] J. Silva, J. W. V. Mello, M. Gasparon, W. A. P. Abrahão, V. S. T. Ciminelli, T. Jong, The role of Al-goethites on arsenate mobility. *Water Res.* **2010**, *44*, 5684. doi:10.1016/J.WATRES.2010.06.056

[33] U. Schwertmann, R. M. Cornell, *Iron Oxides in the Laboratory, Preparation and Characterization*, 2nd edn **2000** (Wiley-VCH: Weinheim, Germany).

[34] D. Leussing, L. Newman, Spectrophotometric study of the bleaching of ferric thioglycolate. *J. Am. Chem. Soc.* **1956**, *78*, 552. doi:10.1021/JA01584A010

[35] S. Brunauer, P. H. Emmett, E. Teller, Adsorption of gases in multimolecular layers. *J. Am. Chem. Soc.* **1938**, *60*, 309. doi:10.1021/JA01269A023

[36] A. C. Larson, R. B. Von Dreele, *General Structure Analysis System (GSAS), Los Alamos National Laboratory Report LAUR 86–748* **1996** (Los Alamos, NM, USA).

[37] B. H. Toby, EXPGUI, a graphical user interface for GSAS. *J. Appl. Cryst.* **2001**, *34*, 210. doi:10.1107/S0021889801002242

[38] A. Szytuła, A. Burewicz, Z. Dimitrijevic, S. Krasnicki, H. Rzany, J. Todorovic, A. Wanic, W. Wolski, Neutron diffraction studies of α-FeOOH. *Phys. Status Solidi B* **1968**, *26*, 429. doi:10.1002/PSSB.19680260205

[39] P. Thompson, D. E. Cox, J. B. Hastings, Rietveld refinement of Debye–Scherrer synchrotron X-ray data from Al_2O_3. *J. Appl. Cryst.* **1987**, *20*, 79. doi:10.1107/S0021889887087090

[40] V. Lenoble, V. Deluchat, B. Serpaud, J. C. Bollinger, Arsenite oxidation and arsenate determination by the molybdene blue method. *Talanta* **2003**, *61*, 267. doi:10.1016/S0039-9140(03)00274-1

[41] W. Stumm, *Chemistry of the Solid–Water Interface: Processes at the Mineral–Water and Particle–Water Interface in Natural Systems* **1992** (Wiley-VCH: Weinheim, Germany).

[42] E. Deschamps, V. S. T. Ciminelli, P. G. Weidler, A. Y. Ramos, Arsenic sorption onto soils enriched in Mn and Fe minerals. *Clays Clay Miner.* **2003**, *51*, 197. doi:10.1346/CCMN.2003.0510210

[43] Y. S. Ho, G. McKay, Pseudo second-order model for sorption processes. *Process Biochem.* **1999**, *34*, 451. doi:10.1016/S0032-9592(98)00112-5

[44] S. E. O'Reilly, D. G. Strawn, D. L. Sparks, Residence time effect of arsenate adsorption/desorption mechanisms on goethite. *Soil Sci. Soc. Am. J.* **2001**, *65*, 67. doi:10.2136/SSSAJ2001.65167X

[45] F. Liu, A. De Cristofaro, A. Violante, Effect of pH, phosphate and oxalate on the adsorption/desorption of arsenate on/from goethite. *Soil Sci.* **2001**, *166*, 197. doi:10.1097/00010694-200103000-00005

[46] J. Antelo, M. Avena, S. Fiol, R. López, F. Arce, Effects of pH and ionic strength on the adsorption of phosphate and arsenate at the goethite–water interface. *J. Colloid Interface Sci.* **2005**, *285*, 476. doi:10.1016/J.JCIS.2004.12.032

[47] J. H. Huang, A. Voegelin, S. A. Pombo, A. Lazzaro, J. Zeyer, R. Kretzschmar, Influence of arsenate adsorption to ferrihydrite, goethite, and boehmite on the kinetics of arsenate reduction by *Shewanellaputrefaciens* strain CN-32. *Environ. Sci. Technol.* **2011**, *45*, 7701. doi:10.1021/ES201503G

[48] C. Hung-Lung, J. Rick, Density function theory: a contemporary perspective for the non-specialist. *Int. J. Appl. Math. Comput. Sci.* **2015**, *2*, 123.

[49] M. Martin, A. Violante, F. Ajmone-Marsan, E. Barberis, Surface interactions of arsenite and arsenate on soil colloids. *Soil Sci. Soc. Am. J.* **2014**, *78*, 157. doi:10.2136/SSSAJ2013.04.0133

[50] B. J. Lafferty, R. H. Loeppert, Methyl arsenic adsorption and desorption behavior on iron oxides. *Environ. Sci. Technol.* **2005**, *39*, 2120. doi:10.1021/ES048701+

[51] J. Cervini-Silva, Alteration of the surface charge of aluminium goethites by a sulfonic acid buffer. *J. Colloid Interface Sci.* **2004**, *275*, 79. doi:10.1016/J.JCIS.2004.01.017

[52] J. van Schuylenborgh, P. Arens, The electrokinetic behaviour of freshly prepared γ-and α-FeOOH. *Recl. Trav. Chim. Pays Bas* **1950**, *69*, 1557. doi:10.1002/RECL.19500691212

[53] G. Bulut, Ü. Yenial, E. Emiroğlu, A. Ali Sirkeci, Arsenic removal from aqueous solution using pyrite. *J. Clean. Prod.* **2014**, *84*, 526. doi:10.1016/J.JCLEPRO.2013.08.018

[54] S. Aredes, B. Klein, M. Pawlik, The removal of arsenic from water using natural iron oxide minerals. *J. Clean. Prod.* **2013**, *60*, 71. doi:10.1016/J.JCLEPRO.2012.10.035

[55] X. Dou, Y. Zhang, B. Zhao, X. Wu, Z. Wu, M. Yang, Arsenate adsorption on an Fe–Ce bimetal oxide adsorbent: EXAFS study and surface complexationmodeling. *Colloids Surf. A Physicochem. Eng. Asp.* **2011**, *379*, 109. doi:10.1016/J.COLSURFA.2010.11.043

[56] S. Goldberg, Application of surface complexation models to anion adsorption by natural materials. *Environ. Toxicol. Chem.* **2014**, *33*, 2172. doi:10.1002/ETC.2566

[57] P. Lakshmipathiraj, B. R. V. Narasimhan, S. Prabhakar, G. BhaskarRaju, Adsorption of arsenate on synthetic goethite from aqueous solutions. *J. Hazard. Mater.* **2006**, *136*, 281. doi:10.1016/J.JHAZMAT.2005.12.015

[58] D. L. Sparks, *Environmental Soil Chemistry* **2003** (Academic Press: New York).

[59] G. P. Jeppu, T. P. Clement, A modified Langmuir–Freundlich isotherm model for simulating pH-dependent adsorption effects. *J. Contam. Hydrol.* **2012**, *129-130*, 46. doi:10.1016/J.JCONHYD.2011.12.001

[60] M. A. Blesa, A. D. Weisz, P. J. Morando, J. A. Salfity, G. E. Magaz, A. E. Regazzoni, The interaction of metal oxide surfaces with complexing agents dissolved in water. *Coord. Chem. Rev.* **2000**, *196*, 31. doi:10.1016/S0010-8545(99)00005-3

[61] A. C. Q. Ladeira, V. S. T. Ciminelli, Adsorption and desorption of arsenic on an oxisol and its constituents. *Water Res.* **2004**, *38*, 2087. doi:10.1016/J.WATRES.2004.02.002